Icarus 258 (2015) 181–191

Contents lists available at ScienceDirect

Icarus

journal homepage: www.elsevier.com/locate/icarus

Giant-planet chemistry: Ammonium hydrosulfide (NH_4SH), its IR spectra and thermal and radiolytic stabilities

Mark J. Loeffler [a,*], Reggie L. Hudson [a], Nancy J. Chanover [b], Amy A. Simon [a]

[a] NASA Goddard Space Flight Center, Greenbelt, MD 20771, USA
[b] New Mexico State University, Department of Astronomy, Las Cruces, NM 88003, USA

ARTICLE INFO

Article history:
Received 19 May 2015
Accepted 11 June 2015
Available online 20 June 2015

Keywords:
Jupiter, atmosphere
Ices, IR spectroscopy
Geophysics
Atmospheres, chemistry
Experimental techniques

ABSTRACT

Here we present our recent studies of proton-irradiated and unirradiated ammonium hydrosulfide, NH_4SH, a compound predicted to be an important tropospheric cloud component of Jupiter and other giant planets. We irradiated both crystalline and amorphous NH_4SH at 10–160 K and used IR spectroscopy to observe and identify reaction products in the ice, specifically NH_3 and long-chained sulfur-containing ions. Crystalline NH_4SH was amorphized during irradiation at all temperatures studied with the rate being the fastest at the lowest temperatures. Irradiation of amorphous NH_4SH at ~10–75 K showed that 60–80% of the NH_4^+ remained when equilibrium was reached, and that NH_4SH destruction rates were relatively constant within this temperature range. Irradiations at higher temperatures produced different dose dependence and were accompanied by pressure outbursts that, in some cases, fractured the ice. The thermal stability of irradiated NH_4SH was found to be greater than that of unirradiated NH_4SH, suggesting that an irradiated giant-planet cloud precipitate can exist at temperatures and altitudes not previously considered.

Published by Elsevier Inc.

1. Introduction

1.1. Background

Theoretical models predict Jupiter's clouds to be mainly NH_3, H_2O, and NH_4SH condensates (Weidenschilling and Lewis, 1973), with NH_4SH believed to come from a thermal reaction between the NH_3 and H_2S that have been detected in the atmosphere (Atreya et al., 1997). Ammonium hydrosulfide (NH_4SH) is also predicted to be an important cloud component of the other giant planets (e.g., Atreya et al., 1999; Roman et al., 2013).

Adequate consideration of NH_3, H_2O, NH_4SH, and their reaction products as contributors to jovian clouds and aerosols and other giant-planet atmospheres requires laboratory studies on these compounds under relevant conditions. However, although ices made of H_2O, NH_3, and mixtures of the two have been studied extensively (e.g., Moore et al., 2007), far less work has been done with NH_4SH. The latter is not commercially available, being unstable to dissociation into NH_3 and H_2S at 298 K. It usually is synthesized through

$$NH_3(g) + H_2S(g) \rightarrow NH_4SH(s) \quad (1)$$

at low temperatures, but the two reactants are toxic, odiferous, and somewhat detrimental to laboratory equipment, perhaps explaining the lack of attention paid to NH_4SH by experimentalists.

Vapor pressure measurements of NH_4SH were first reported by Isambert (1881), a melting point was published by Briner (1906), and crystallographic studies were done by West (1934). The first published infrared (IR) spectra of solid NH_4SH were from Bragin et al. (1977), who identified the strongest mid-IR absorptions as being near 3000, 1830, 1400, and 470 cm^{-1} (~ 3.3, 5.5, 7.1, and 21 μm) for the crystalline solid near 100 K. A different NH_4SH ice was reported to have broad IR absorptions, and subsequent work by Ferraro et al. (1980) identified this solid as amorphous NH_4SH, with the amorphous-to-crystalline phase change being near 160 K. Nearly 30 years later the IR optical constants of NH_4SH were published by Howett et al. (2007). Work in other spectral regions is limited to the electronic spectra of Lebofsky and Fegley (1976), who reported that the ultraviolet–visible reflectance spectrum of NH_4SH is relatively featureless and flat, albeit with a slight rise from 300 to 1000 nm (slight red slope).

Ices made only of pure NH_3, H_2S, and NH_4SH lack strong absorptions in the visible region and cannot be the source of jovian colors. However, since Jupiter's atmosphere is subject to energetic particle bombardment and solar-UV photolysis, all cloud components will undergo chemical changes with possible alterations of color, and

* Corresponding author.

http://dx.doi.org/10.1016/j.icarus.2015.06.015
0019-1035/Published by Elsevier Inc.

such changes lend themselves to laboratory experiments. Indeed, conference abstracts highlighting such work are available spanning 30 years (Bragin and Chang 1976; Huntress and Anicich, 1984; Delitsky and Baines 2007), but detailed studies of solid NH_4SH in the refereed literature are surprisingly scarce, and one still encounters publications calling for new investigations into the chemistry of NH_4SH (e.g., de Pater et al., 2001; Howett et al., 2007) and the $NH_3 + H_2S$ system (Wong et al., 2015).

The most-relevant laboratory work on NH_4SH chemistry is from Lebofsky and Fegley (1976), who photolyzed ices made of NH_3, H_2O, H_2S, and NH_4SH at 77 K with a filtered xenon lamp, whose output at 220–300 nm served as an analog to the solar flux. Reflectance spectra from 300 to 1000 nm of NH_3 and H_2O hardly changed with photolysis, but a strong absorption was produced near 600 nm for H_2S and NH_4SH ices and was assigned to sulfur radicals. In addition, photolysis changed the nominally featureless reflection spectra of H_2S and NH_4SH to spectra that sloped downward from 700 to 300 nm, suggesting an absorber outside the range of wavelengths studied. No temperature variations or kinetic studies were reported.

In addition to the lack of relevant laboratory work, many of the relevant observational spectra are derived from the Hubble Space Telescope images that have a gap near the 600-nm absorption (Strycker et al., 2011), making comparisons to laboratory spectra even more difficult. At the least this all suggests that a much more detailed study of NH_4SH and its thermal, photochemical, and radiation chemical stabilities is warranted, keeping in mind that multiple components may be needed explain the color variations observed in Jupiter's atmosphere (Simon-Miller et al., 2001; Strycker et al., 2011).

1.2. Our approach

This paper describes our recent laboratory work focused on NH_4SH, particularly its IR spectra and reaction chemistry. A novelty of our approach is its use of radiation-chemical methods. Whitten et al. (2008) suggested that jovian clouds will be altered more by cosmic rays than solar photons since the latter will not penetrate deeply into the atmosphere. Therefore, to initiate reactions in NH_4SH we use ionizing radiation in the form of ~1 MeV protons (p+), which are an analog to the low-energy, and more-abundant, cosmic rays. To first order the products of UV-photochemistry and radiation chemistry are the same (e.g., Hudson and Moore, 2001; Baratta et al., 2002), but our radiation-chemical approach permits the use of thicker samples than in conventional photochemistry, which in turn allows the detection of weaker IR features.

Some topics of specific interest here are the possible persistence of IR absorptions of NH_4SH after proton bombardment, the temperature dependence of any such spectral features, and whether assignments can be made to IR absorptions of chemical products. Here we present results on both of the reported phases of NH_4SH under vacuum from 10 to over 200 K. During the radiation experiments, each sample was monitored with IR spectroscopy and mass spectrometry to determine stability and chemical change as a function of temperature and radiation dose. The results of such measurements can serve as an important link between the IR region, which is sensitive to chemical composition and phase, and the ultraviolet–visible observations of Jupiter.

2. Experimental

Much of the experimental approach is as described in Loeffler et al. (2011), but a few points require additional comments.

2.1. Equipment and synthetic methods

Gases used (and purities) to prepare and study NH_4SH were NH_3 from Matheson (99.9992%), $^{15}NH_3$ from Cambridge Isotopes (98%+), and H_2S from Matheson (99.5%). All reagents were used as received. Indices of refraction (n) were needed to calculate thicknesses of samples made from these reagents. For NH_3, we used $n = 1.48$ from Romanescu et al. (2010) and $n = 1.49$ for H_2S (liquid, Weast et al., 1984). Thicknesses of ice samples were 1.2 μm unless otherwise stated and were calculated from densities of 0.81 g cm^{-3} for NH_3 and 1.17 g cm^{-3} for H_2S and an assumption of uniform mixing.

Experiments were performed with a stainless steel high-vacuum chamber ($P < 1 \times 10^{-7}$ Torr) interfaced with a cryostat ($T_{min} \sim 10$ K) and gas-handling system. Ammonium hydrosulfide (NH_4SH) was synthesized *in situ* by co-deposition of H_2S and NH_3 gases from two separate lines onto a pre-cooled (10–90 K) substrate attached to the cryostat's cold-finger. The deposition rate of each gas was calibrated as in Loeffler et al. (2011) to ensure that the initial composition of each ice was known. Although a 1:1 stoichiometric ratio applies for the reaction $NH_3(g) + H_2S(g) \rightarrow NH_4SH(s)$, an initial ratio closer to 1.2:1 = NH_3:H_2S was found to minimize the excess reactants for a mixture deposited at 50 K. Substrates made of unpolished aluminum, gold-coated unpolished aluminum, and gold-coated polished aluminum were used, with only the last one being considered optically flat. The spectra of Fig. 1 were recorded on the gold-coated polished aluminum substrate, but all others shown were with a gold-coated unpolished aluminum substrate. In general, the results in this paper were independent of the substrate employed.

After deposition of the reactant gases, the resulting solid-phase mixture was warmed to 120 K at 2 K min^{-1} to obtain amorphous NH_4SH and to 155 K to obtain a crystalline sample. Crystallization of NH_4SH began near 130 K, and sublimation into the vacuum occurred in a few minutes at 170 K. These temperatures were somewhat sensitive to the substrate's cleanliness, so after each radiation experiment the substrate was wiped with CS_2 to remove any sulfur residue that may have formed, followed by wiping with acetone. Material, if any, released from ices during irradiation was monitored with a Dycor DM300 mass spectrometer, with a dwell time of 120 ms on each peak selected. Samples prepared for irradiation were grown at 90 K to minimize the

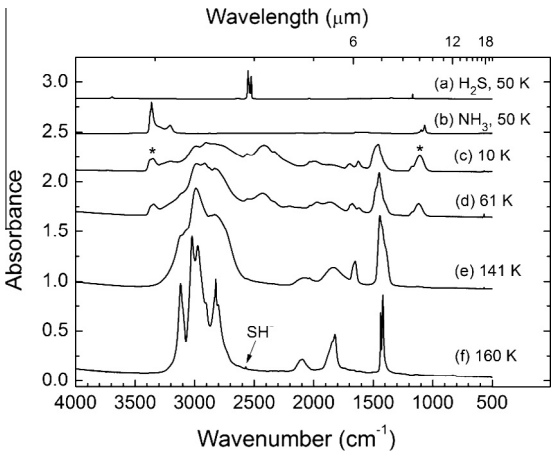

Fig. 1. Reference spectra of (a) H_2S and (b) NH_3 ices deposited at 50 K compared to spectra of a $H_2S + NH_3$ (1:1) mixture (c) deposited at 10 K and then (d)–(f) warmed to 160 K at 2 K min^{-1}. The spectra of the H_2S and NH_3 samples have been scaled by 0.25. The 141 K spectrum corresponds to amorphous NH_4SH and that at 160 K to crystalline NH_4SH. Asterisks (*) indicate features from NH_3. Spectra in this and other figures have been offset for clarity.

abundances of potential contaminants trapped in the ice during gas-phase deposition of NH_3 and H_2S.

2.2. Irradiation techniques

Ices were irradiated with ~1 MeV protons (p+) from a Van de Graaff accelerator following the methods of Loeffler et al. (2011), except that a different beam foil, separating the vacuum systems of the cryostat and accelerator, was installed. New calibrations of the resulting p+ energy at our substrates, using a Si detector placed in the position of an ice sample, showed that the energy of 1.03 MeV protons was reduced on average to 0.924 MeV after passing through the foil, with a full width at half maximum of 0.034 MeV. These incident 0.9 MeV protons passed through our NH_4SH ice samples, which allowed measurement of the incident dose (fluence in p+ cm^{-2}) by integrating the current on the underlying metal substrate in real time and dividing by the area of the ion beam on the sample (4.85 cm^2). Using SRIM2010 (Ziegler, 2010), the energy loss for a 0.924 MeV p+ passing through NH_4SH was found to be 0.0285 MeV μm^{-1}, assuming a density of 1.18 g cm^{-3} (West, 1934). Conversions to other units are as follows: 1.00×10^{14} p+ cm^{-2} fluence = 2.05 eV molecule^{-1} = 3.87 MGy = 387 Mrad. Samples were biased at +35 V to minimize the loss of secondary electrons. The proton beam current typically was 100 nA, for an incident dose rate of about 1.3×10^{11} p+ cm^{-2} s^{-1} in NH_4SH.

2.3. Analytical technique and data analysis

Infrared spectra of ices were measured as in Loeffler et al. (2011) with a resolution of 2 cm^{-1} and using 120 scans per spectrum. Most spectra were acquired from 8000 to 500 cm^{-1}, but recently we have been able to extend this range down to near 350 cm^{-1}, which is reflected in some of the spectra shown here. For amorphous ices, whose absorption features did not change shape significantly during irradiation, we measured the integrated intensity $\mathcal{A}$ of each IR band of interest, with $\mathcal{A}$ defined by

$$\mathcal{A} = \int Abs(\tilde{\nu}) d\tilde{\nu} \quad (2)$$

for an absorbance scale. Before measuring $\mathcal{A}$, we subtracted a baseline that best matched the continuum on each side of an IR feature, which in most cases was a straight line. For crystalline NH_4SH, whose absorptions changed shape dramatically during irradiation (broadening), we evaluated the sample's crystallinity by studying the peak-to-peak change in the first-derivative spectrum (Chestnut, 1977). Finally, in each experiment we normalized band areas (or peak heights) by dividing by the initial area (or height) of the relevant IR feature of the unirradiated sample. This facilitated comparison of results from experiments with ices of different thicknesses.

3. Results

3.1. Synthesis and spectroscopy of NH_4SH

Before presenting new results, it is important to verify our agreement with previous work on the synthesis and spectra of NH_4SH. Traces (a) and (b) of Fig. 1 are the mid-IR spectra of H_2S and NH_3, respectively, near 50 K. The spectrum of an amorphous mixture of H_2S + NH_3 (55:45) that was condensed at 10 K is shown in (c), while (d) is after warming to 61 K. Comparing (a) through (d) it is clear that new IR features are present in the spectrum of the two-component ice mixture that belong to neither H_2S nor NH_3. These new features, present even at 10 K, agree with those found in the only published spectrum of amorphous NH_4SH (Ferraro et al., 1980), indicating that some of our H_2S and NH_3 reacted on deposition. Raising the deposition temperature increased the amount of NH_4SH initially formed. Warming ice mixtures made below 90 K produced identical spectra of pure amorphous NH_4SH at 120–140 K, with the temperature range being a function of time, deposition temperature, heating rate, and substrate. Traces (e) and (f) of Fig. 1 show further spectral changes as the sample was warmed, corresponding to the complete formation of (e) amorphous and (f) crystalline NH_4SH. Crystallization began at 130–150 K with the range being somewhat sensitive to the preparation conditions. When heating our initial two-component mixture to form amorphous and crystalline NH_4SH, we typically would leave the sample at the highest temperature until the IR spectra stopped changing, which usually was less than about 20 min.

Of the NH_4SH spectral features in Fig. 1, the strong peak near 1445 cm^{-1}, assigned to a deformation vibration of NH_4^+, is the most important for this paper. Changes in the integrated intensity of this IR band will be used to follow radiation-induced destruction of NH_4SH. Here we also remind the reader that NH_4SH is an ionic compound and so there are no molecules of NH_4SH present in our solids, only NH_4^+ and HS^- ions. See Fig. 1 of Bragin et al. (1977) for an illustration of the unit cell of crystalline NH_4SH based on the work of West (1934).

Several observations argue for a high purity of our NH_4SH ices. First, each spectral feature of NH_4SH was in its expected position in both phases, and no features were evident for common laboratory contaminants such as solid-phase H_2O (3300, 1600 cm^{-1}) and CO_2 (2343 cm^{-1}). In addition, IR peaks from the starting materials fell nearly to the level of the spectral noise on heating the initial H_2S + NH_3 mixture. For instance, in Fig. 1 we estimate that during heating to the amorphous phase (e) the NH_3 features drop by over a factor of twenty and at least another factor of two on reaching the crystalline phase (f). Considering that some of the starting material has already reacted upon deposition, these observations suggest that the amorphous sample is >95% pure, while the crystalline is likely closer to 99%. In short, our spectra appear to be for the purest NH_4SH yet reported.

With so few spectroscopic papers related to NH_4SH available, only a few comparisons of our work with the literature are possible. The earliest IR work appears to be that of Bragin et al. (1977) who showed a single spectrum at 98 K of the crystalline solid. Aside from it having a few small extra absorptions at 1750–1500 cm^{-1}, and showing traces of trapped NH_3, that spectrum agrees with our Fig. 1(f). Ferraro et al. (1980) later published two IR spectra of NH_4SH, one for the amorphous solid at 89 K and one for the crystalline ice at 160 K. Water–vapor features obscured the 1700 cm^{-1} region at 160 K, and both spectra showed that the ices contained residual NH_3, but otherwise those two spectra match what is shown in our Fig. 1. The only other IR study of NH_4SH seems to be that of Howett et al. (2007), who published optical constants, but no spectra. We will return to their results in our Discussion section.

3.2. Radiation-chemical destruction of NH_4SH

In presenting our radiation-chemical results we begin with crystalline NH_4SH. Fig. 2 shows changes in the IR spectra of crystalline NH_4SH caused by successive irradiations at 50 K with 0.9 MeV p+. The sharp absorption features in 2(a) decreased and broadened with increasing dose, changes that we assign to the radiation-induced amorphization of the sample. The crystalline fraction (f_C) of each NH_4SH ice was followed by monitoring the decrease in intensity of the compound's small, but sharp, SH^- band at 2570 cm^{-1}, which was reduced to almost zero during irradiation. The top panel of Fig. 3 summarizes data from six experiments

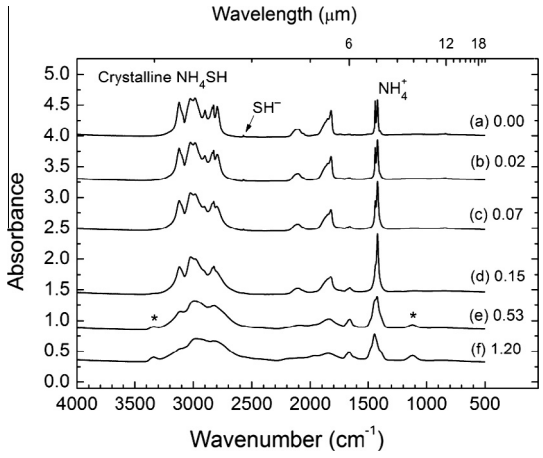

Fig. 2. Infrared spectra of crystalline NH_4SH after successive irradiations at 50 K. The accumulated incident dose (fluence in 10^{15} p+ cm^{-2}) is given to the right of each spectrum, and asterisks (*) indicate features from NH_3. The sample used for (a) was made by depositing the reactant gases at 90 K, warming to 155 K to crystallize the solid, and then cooling to 50 K for irradiation. Spectra are offset for clarity.

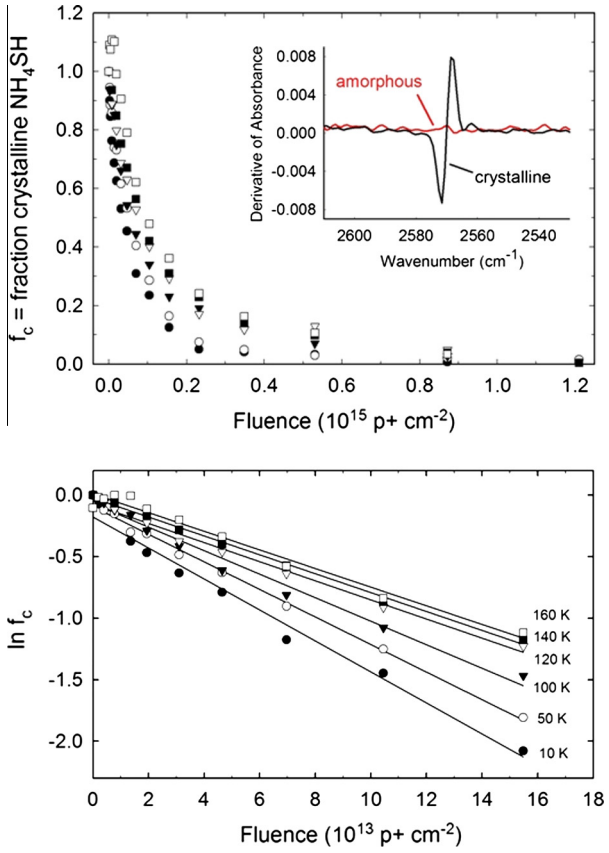

Fig. 3. Radiation-induced amorphization of crystalline NH_4SH as a function of temperature. The upper panel shows the loss of crystallinity for six temperatures, with an insert showing the first-derivative of the SH^- band measured. The lower panel shows first-order kinetics plots for the amorphization at low doses.

and shows the fall of the SH^- feature's intensity, specifically the peak-to-peak amplitude of its first-derivative spectrum shown in the insert. The curves decrease substantially at high doses and are subject to greater uncertainties there than in the early stages of the irradiation. The relatively small amount of crystalline reactants remaining at the end of each experiment ($f_C \approx 0$) means that reactions to recrystallize the NH_4SH ice can be ignored initially. Treating the early part of each decay curve with first-order kinetics (exponential decay) gives the lower panel of Fig. 3, with each line's slope being the negative of the rate constant k for destruction of crystalline NH_4SH. Numerical values of k will be given in the Discussion section.

Since spectral changes caused by irradiating crystalline NH_4SH could come from either amorphization or molecular destruction, nearly all of the remaining results we present are for amorphous ices. However, amorphous samples were not irradiated above 120 K because they would have begun to crystallize, complicating the analysis of the results. Fig. 4 shows changes to the IR spectrum of amorphous NH_4SH caused by successive irradiations at 50 K with 0.9 MeV p+. The loss of NH_4SH is seen with increasing dose (fluence, p+ cm^{-2}) and NH_3 production is indicated by the appearance of that molecule's absorptions at 3339 (ν_1, ν_3) and 1120 cm^{-1} (ν_2). The growth of weak bands below 700 cm^{-1}, shown in detail later, also was noted as were subtle changes at 2600–2400 cm^{-1} that could be from H_2S formation. The close similarity of Figs. 2(f) and 4(f) shows that the reaction products from the two phases of irradiated NH_4SH were the same, as expected.

Fig. 5 shows the decrease in band area, $\mathcal{A}$, of our compound's strong 1445 cm^{-1} NH_4^+ feature as a function of both temperature and dose. Two distinct types of decay were observed, one for 75 K and below (lower panel), in which an equilibrium plateau was reached, and the other type for 100 K and above (upper panel), in which it was not. At 75 K and below, the decay was faster at the lower temperatures and led to an equilibrium normalized abundance, $\mathcal{A}/\mathcal{A}_0$, of ~0.5 at 10 K and ~0.75 at 50–75 K. At 100 K, the NH_4^+ decay curve's concavity resembles that seen at lower temperatures, indicating that the sample may be approaching equilibrium, although the projected equilibrium band area is much smaller than at the lower temperatures. Furthermore, it appears that at very low p+ doses there is almost no decrease in band area. These differences for the 100 K irradiations were even more pronounced in our 120 K experiments. The initial change in NH_4^+ band area at 1445 cm^{-1} was small until $\sim 1 \times 10^{14}$ p+ cm^{-2}, or about 10% of the total dose, was reached. After that, the decay data was fit reasonably well with either a straight line or an exponential function that approaches 0.

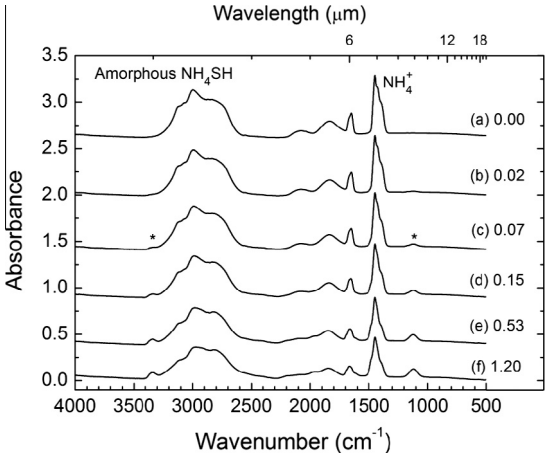

Fig. 4. Infrared spectra of amorphous NH_4SH after successive irradiations at 50 K. The accumulated incident dose (fluence in 10^{15} p+ cm^{-2}) is given to the right of each spectrum. Asterisks (*) indicate features from NH_3. The sample used for (a) was made by depositing the reactant gases at 90 K, warming to 120 K to make amorphous NH_4SH, and then cooling to 50 K for irradiation. Spectra are offset for clarity.

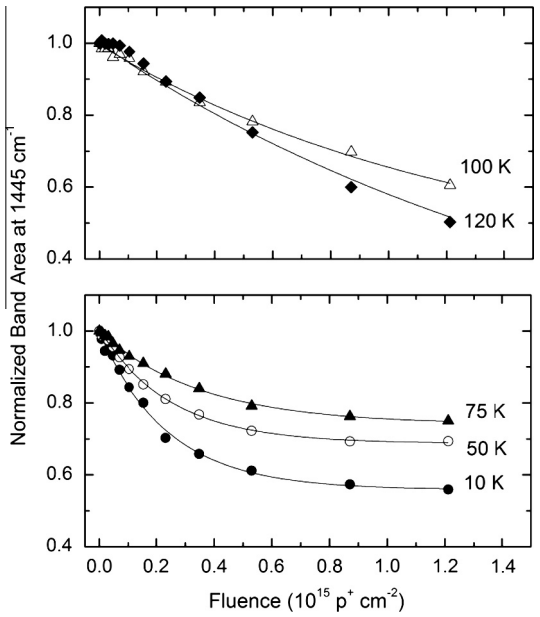

Fig. 5. Decrease in normalized band intensity, A/A_0, of the 1445 cm^{-1} NH_4^+ absorption during the irradiation of amorphous NH_4SH.

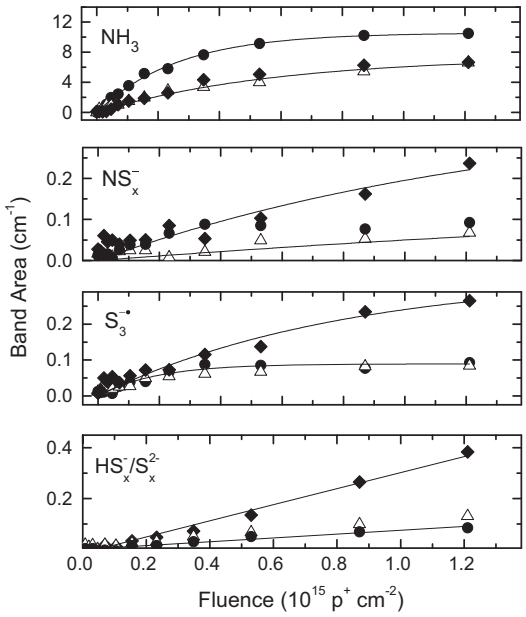

Fig. 7. Increase in the NH_3 (1120 cm^{-1}), NS_x^- (682 cm^{-1}), $S_3^{-\cdot}$ (565 cm^{-1}) and S_x^{2-}/HS_x^- (491 cm^{-1}) absorptions during irradiation of amorphous NH_4SH at 10 (•), 75 (Δ), and 120 K (♦). The lines are to guide the eye.

3.3. Radiation-chemical products from NH_4SH

Although we are concerned with the radiolytic stability of NH_4SH ices, we also documented spectral changes of reaction products. Our IR methods give information about solids by *in-situ* analysis, but since many possible reaction products of NH_4SH absorb in the same region, from about 1000 to 400 cm^{-1} in this case, it can be difficult to make unique assignments. Along these lines, irradiated NH_4SH produced not only NH_3 but also new products with IR bands near 682, 566, and 491 cm^{-1}, which we have identified as most likely being due to NS_x^-, $S_3^{-\cdot}$ and S_x^{2-}/HS_x^- respectively (see Section 4.3). Fig. 6 shows the growth of these three weak IR features in a 2.1 μm thick NH_4SH sample irradiated at 120 K. The four panels of Fig. 7 record the growth of these same absorptions, and also one of NH_3 (1120 cm^{-1}), at multiple temperatures. The abundance of NH_3 was greatest at the lowest temperature, perhaps because some of the synthesized NH_3 sublimated from the ice after it was produced at ~100 K and above. The three other sulfur product bands had the opposite behavior, being about three to four times more abundant at the higher temperatures than the lower ones. Furthermore, at the higher temperatures none of these three weak bands had reached equilibrium by the final irradiation.

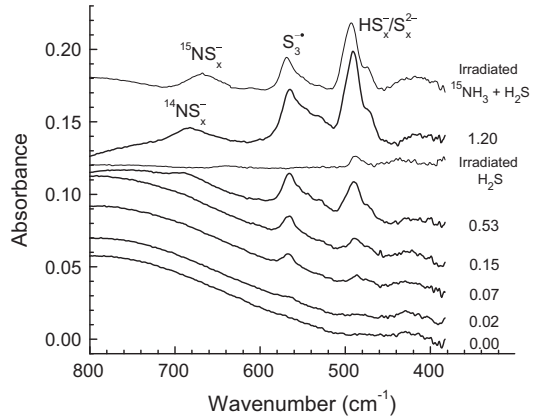

Fig. 6. From bottom to top, IR spectra of amorphous NH_4SH at 120 K after the radiation doses (fluences, 10^{15} p+ cm^{-2}) given at the right. The initial thickness of the NH_4SH sample before irradiation was 2.1 μm. For comparison, a spectrum of amorphous H_2S irradiated at 75 K also is shown.

3.4. Post-irradiation heating

The upper panel of Fig. 8 shows IR spectra of an amorphous NH_4SH sample that was irradiated at 120 K to 1.2 × 10^{15} ions cm^{-2} and then warmed at 0.4 K min^{-1}. Significant spectral changes were first observed near 180 K when the NH_4^+ feature near 1445 cm^{-1} began to sharpen slightly, perhaps suggesting the onset of crystallization. However, the other main spectral bands hardly changed, unlike what we observed with the unirradiated sample (Fig. 1).

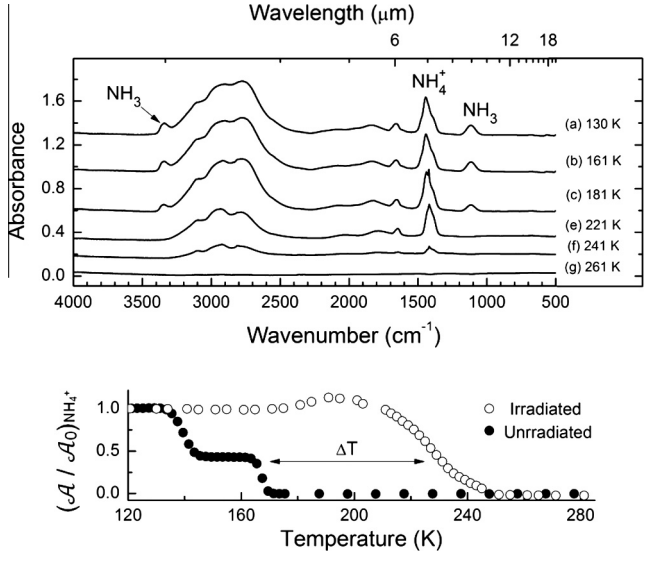

Fig. 8. Upper panel: IR spectra recorded on warming amorphous NH_4SH that had been irradiated at 120 K to a fluence of 1.2 × 10^{15} p+ cm^{-2}. Very weak features at 261 K are from an absorption on the KBr window of the sample chamber. Lower panel: Changes in the normalized band area of the 1445 cm^{-1} NH_4^+ absorption on warming unirradiated and irradiated amorphous NH_4SH samples at 0.4 K min^{-1}. The irradiation was to a fluence of 1.2 × 10^{15} p+ cm^{-2} at 120 K.

For example, no sharpening of the broad SH^- band near 2570 cm^{-1} was seen on warming irradiated NH_4SH.

Monitoring the IR bands of the new products during warming showed that each band had a different temperature dependence. The absorption peak of the S_3^-· radical (566 cm^{-1}) dropped to the noise level by ~175 K and the peak assigned to NS_x^- (682 cm^{-1}) did the same by 200 K. Infrared absorptions from NH_3 began to decrease near 180 K and were undetectable by 200 K. Other experiments (e.g. Fig. 6), with our extended spectral range, showed that the S_x^{2-}/HS_x^- feature (491 cm^{-1}) showed similar thermal behavior as the NH_4^+ features (e.g., near 2900, 1450 cm^{-1}), persisting until the entire sample began to sublimate.

The lower panel of Fig. 8 shows the change for the NH_4^+ ion in a more-quantitative manner. The normalized area, $\mathcal{A}/\mathcal{A}_0$, of the 1445 cm^{-1} NH_4^+ absorption was measured on warming unirradiated amorphous NH_4SH and then compared to the intensity changes for the same IR band in a sample irradiated at 120 K. For the unirradiated sample, the band area remained relatively constant until near 140 K, where it dropped to 40% of its original value, then stayed relatively constant until about 160 K, and then made a final decrease toward the baseline (noise level), which it reached by ~170 K. The corresponding IR spectra showed that the initial drop was from crystallization of the sample, and an accompanying sharpening of the NH_4^+ absorption, while the second decrease was from rapid sublimation (decomposition) of NH_4SH.

In contrast to these changes, Fig. 8 also shows that warming a proton-irradiated NH_4SH sample gave a small increase in the NH_4^+ feature's intensity, perhaps from thermal annealing of the sample or perhaps from recombination of radiolysis products to again make NH_4SH. No decrease in the NH_4^+ band area was seen near 140 K that would correspond to crystallization, which agrees with the lack of sharp features in the IR spectra at higher temperatures. The only drop seen in the NH_4^+ band's area for irradiated samples is likely due to the onset of sublimation, which began near 200 K and above which all absorptions decreased until the noise level was reached at ~250–260 K. Fig. 8 clearly shows that irradiation of NH_4SH raised the thermal stability of the solid sample by $\Delta T \sim 70$ K.

3.5. Gases released during irradiation

During irradiation of amorphous NH_4SH at 100 K and above, we observed large pressure spikes in the readings from the mass spectrometer and ionization gauge attached to our vacuum system. These spikes appeared to have been from the explosive release of material from the sample. In the most extreme cases these bursts were sufficiently great that the filaments in both instruments would shut off due to the large amount of material released. An example of what we observed for $m/z = 34$, the H_2S^+ channel of the mass spectrometer, is shown in Fig. 9 for a sample irradiated at 120 K. The result from a 75-K irradiation, which displayed no outbursts, is shown for comparison. The large spikes in the H_2S^+ signal were accompanied by outbursts in other channels that corresponded to the ions (m/z values) N^+ (14), NH^+ (15), NH_3^+ (17), S^+ (32), and HS^+ (33), each an expected fragmentation product of NH_4SH, NH_3, or H_2S. Pressure spikes for H_2^+ were observed but with more difficulty as they were superimposed on a high steady flux that increased with radiation dose. No spikes corresponding to N_2^+ were observed, and no outburst was expected, or seen, for NH_4SH^+ as it decomposes in the gas phase. Visual inspection of a thicker irradiated NH_4SH sample after a pressure burst showed it to be fractured or, in some of the more extreme cases, missing from part of the underlying metal substrate, an observation made with multiple NH_4SH ices. No pressure outbursts were observed either from unirradiated NH_4SH, NH_3, or H_2S on warming, or from NH_3 or H_2S samples irradiated at 75 K. Experiments showed that the outbursts were seen much more readily for irradiated amorphous NH_4SH than for irradiated crystalline NH_4SH.

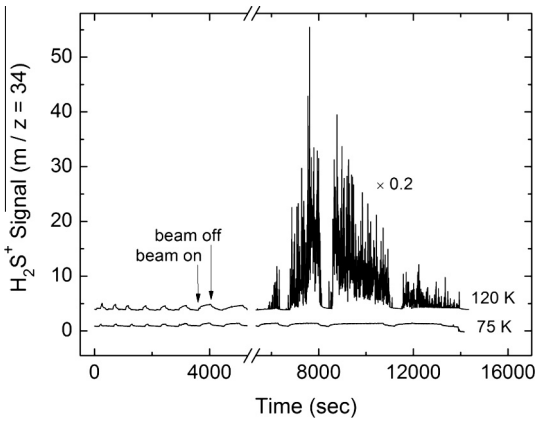

Fig. 9. Mass spectrometer signal for H_2S^+ ($m/z = 34$) during irradiation of amorphous NH_4SH at 75 and 120 K. The small rises and falls in signal, seen most clearly before about 5000 s, correspond to the proton beam being turned on and then off so that an IR spectrum could be recorded. In the 120 K experiment, the y-axis values (H_2S^+ signal) after about 5000 s have been multiplied by 0.2 to bring them onto the scale of the figure. The flux throughout the experiment was about 1.3×10^{11} p+ cm^{-2} s^{-1}. Traces have been vertically offset for clarity.

Although these pressure bursts and their importance are still under investigation, we already can make several general observations about them. The peak intensity of the bursts varied among our experiments, but the proton fluence (dose) at which the bursts first appeared was always the same within roughly a factor of two. Lowering the irradiation rate by a factor of three did not stop the bursts from occurring. At low fluences, the mass spectrometer signals were similar in shape for 100 and 120 K irradiations, but the 120-K irradiation gave bursts roughly twice as intense as those at 100 K. Although bursts were seen at temperatures as low as 100 K, at 100 K they began after a higher proton fluence. They also were somewhat more sudden on a polished mirror substrate than on an unpolished one. For the sample irradiated at 120 K, bursts began after about 2×10^{14} ions cm^{-2} and reached a peak near 4×10^{14} ions cm^{-2}; these same outbursts decreased in intensity as the experiment progressed, but typically could still be seen through the final irradiation.

3.6. Other experiments

Besides these experiments to study the chemistry and spectroscopy of NH_4SH, we undertook a preliminary examination of changes in sample thickness during an irradiation. It is well known that a solid can experience erosion of its surface during radiolysis, a process known as sputtering. Complicating this effect is that sample loss can also occur in our irradiated NH_4SH from both sublimation of material and from chemical reactions. Losses from sublimation can be controlled, or at least accounted for, by a careful choice of temperature while independent checks at low temperature can reveal the extent of chemical loss. However, at higher temperatures both effects are operative as is the removal of material by sputtering, raising questions about the shapes and underlying causes of decay curves such as those of Fig. 5. In short, the curves of Fig. 5 clearly indicate sample loss, but by which mechanisms?

The two panels of Fig. 10 are for an experiment different from those already presented. It has long been known that the Beer's Law linear relationship between the sample thickness and the absorbance of light fails for thin films (e.g., Maeda and Schatz, 1961; Fujiyama et al., 1970) and such failures can be especially severe for spectra recorded by reflection off of metals (Pacansky

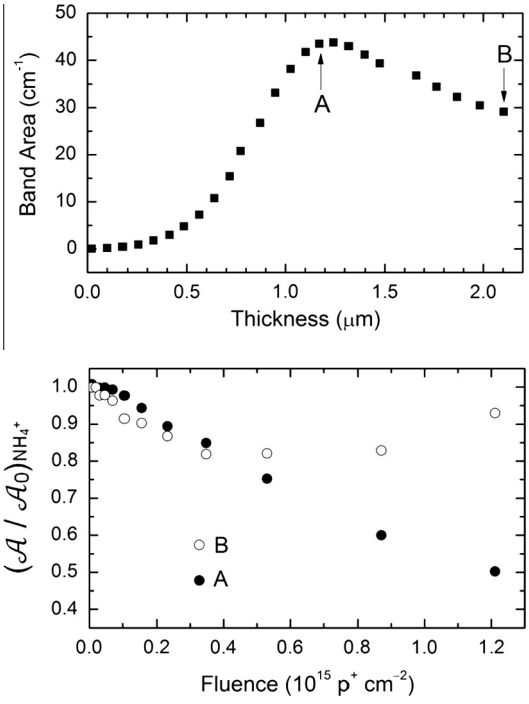

Fig. 10. The upper panel shows the area of the 1445-cm^{-1} band of NH_4^+ as a function of NH_4SH thickness. The lower panel shows the change in the same band's area during irradiation of amorphous NH_4SH samples initially having the thicknesses A (1.2 μm) and B (2.1 μm) indicated in the upper panel.

and England, 1986; Teolis et al., 2007). The upper panel of Fig. 10 illustrates this, the data being measurements of the integrated absorbance $\mathcal{A}$ of the NH_4^+ ion's absorption at 1445 cm^{-1} (λ = 6.920 μm) for different thicknesses of amorphous NH_4SH. Clearly there are thicknesses above ~1.2 μm where a *decrease* in the ice's thickness, such as due to radiation-induced loss of material, could produce an *increase* in a spectral absorbance. To investigate whether such an effect might be seen with our irradiated ices, and influence our measurements, we prepared two NH_4SH samples of different thicknesses and irradiated them. The lower panel of Fig. 10 shows the absorbance changes produced by irradiating these ices having thicknesses of ~1.2 μm (A) and ~2.1 μm (B); we will return to these results in Section 4.5.

4. Discussion

4.1. Spectroscopy of NH_4SH ices

The IR spectra of our unirradiated amorphous and crystalline NH_4SH (Fig. 1) are in qualitative agreement with the three published spectra, one for the amorphous solid and two for the crystalline, but a more quantitative comparison is desirable. Unfortunately, the IR spectrum of Bragin et al. (1977) has a vertical axis with a numerical scale, but no ice thicknesses were provided, while the spectra of Ferraro et al. (1980) are accompanied with ice thicknesses, but no vertical scales with numbers. Therefore, quantitative comparisons of our NH_4SH spectra with these earlier ones are impossible.

Another approach to a literature comparison is to use the work of Howett et al. (2007) who published optical constants for NH_4SH. However, no IR spectra were shown and few details were given about the authors' method to convert optical constants to spectra. We used two different methods (Hudson et al., 2014) to compute NH_4SH spectra from the constants of Howett et al. (2007), but the relative band intensities given by our calculations did not agree with either our own spectra in Fig. 1 or with the spectra published by others (Bragin et al., 1977; Ferraro et al., 1980). We are investigating these discrepancies.

4.2. Amorphization of crystalline NH_4SH

One new finding in this paper is the structural change produced by ion irradiation of crystalline NH_4SH, a presumed cloud component of the gas-giant planets. It is clear from Fig. 2 that irradiation destroys the sharp absorption features indicative of a crystalline material, leaving behind a solid that has little structural order. However, we point out that the composition of the sample has also been altered by irradiation, as the solid is now composed of new radiation products, as well as the original material, and most closely resembles the spectrum of the irradiated amorphous NH_4SH. Thus the values given for the amorphization rate constants (k) for the six temperatures of Fig. 3 (Table 1) inevitably are a combination of structural and chemical destruction of the ice sample. The contribution from the chemical destruction, which is clearly important at all temperatures studied here, is likely why the k value does not change significantly with temperature. For comparison, the k value for the more chemically stable H_2O–ice drops by ~100 on going from 36 to 77 K (Moore and Hudson, 1992; Strazzulla et al., 1992).

4.3. Radiation products

The three labeled peaks from irradiated NH_4SH shown in Fig. 6 are in an IR region of SS stretching and SSS bending vibrations, making us confident that we have observed the radiation synthesis of polysulfur species. The observation that each peak has different temperature dependence argues strongly for the formation of at least three sulfur-containing reaction products in irradiated NH_4SH. The ~70 K rise in stability for NH_4^+, illustrated in Fig. 8, is consistent with the three features being more-complex species than HS^-.

While irradiation of pure NH_3 ices yielded no new IR features in the region of our new product bands, irradiation of pure H_2S did give an IR peak at 491 cm^{-1} (Fig. 6). Irradiation of H_2S is known to produce H_2S_x molecules, which have strong S–S stretches in the 500–400 cm^{-1} region (Wieser et al., 1969). In our irradiated NH_4SH, the NH_3 formed will convert these hydrosulfides to HS_x^- or S_x^{2-} with similar IR positions (Janz et al., 1976; Steudel, 2003). An assignment of our 491-cm^{-1} feature to one or more of these ions is favored. The least thermally stable of the three product peaks in Fig. 6 was the one at 566 cm^{-1}. Its position is reasonably close to that of the relatively unstable anion radical $S_3^{-\cdot}$, which is known to form in reactions of sulfur in liquid NH_3 (Dubois et al., 1988), and both sulfur and NH_3 are expected in irradiated NH_4SH. Sulfur reacting in condensed NH_3 also forms NS_4^- and NS_3^- with a strong IR band near 700 cm^{-1} (Dubois et al., 1987) and a ^{15}N isotopic shift of 14 cm^{-1} (Chivers et al., 1980), the same as in our $^{15}NH_4SH$ work, which is shown in Fig. 6 for comparison.

Table 1
Radiation-induced amorphization of crystalline NH_4SH.

T (K)	k (cm^2/p+)/10^{-15}
160	7.6
140	7.7
120	7.8
100	9.6
50	11.2
10	12.6

Each entry for k is from a least-squares fit of the data to an exponential decay of the form $y = e^{-kF}$, where y is the fraction of crystalline NH_4SH present after proton fluence F (p+ cm^{-2}) and k is the decay constant. See Fig. 3 and the text for additional information.

Thus, we assign our 682-cm^{-1} band to an ion, or ions, of the form NS_x^-.

4.4. Radiation chemistry of NH_4SH

We are unaware of any previous radiation-chemical studies of NH_4SH, and the only photochemical study appears to be that of Lebofsky and Fegley (1976), whose experiments were at a single temperature and used electronic spectroscopy. Lacking prior work with which to understand NH_4SH radiation chemistry, we instead consider ion irradiations of related compounds for insight.

As already stated, ammonium hydrosulfide is not made of NH_4SH molecules, but rather of ammonium (NH_4^+) and bisufide (SH^-) ions. It is with these ions that the initial radiation-driven changes in NH_4SH will take place. Changes expected for NH_4^+ can be predicted from the radiation chemistry of the isoelectronic methane (CH_4) molecule. Exposure of solid CH_4 to ionizing radiation, such as our p+ beam, produces tracks of ionizations and excitations through the sample from the thousands of secondary electrons generated by the incident radiation. Two expected reactions are

$$CH_4 \rightarrow CH_4^* \rightarrow CH_3 + H \quad (3)$$

$$CH_4 \rightarrow CH_4^* \rightarrow CH_4^+ + e^- \quad (4)$$

giving both charged and neutral radicals. For NH_4^+ these same types of reactions will produce $(NH_4^+)^*$ which will dissociate as with (3) to give NH_3^+, the nitrogen counterpart of the CH_3 radical, and a hydrogen atom. Although CH_3 is one of the more-reactive organic radicals, NH_3^+ is expected to be retained in our ices even up to 170 K (Cole, 1961; Hyde and Freeman, 1961). Reaction (4) suggests that NH_4^{2+} also will form in proton-irradiated NH_4SH. However, unlike the case of irradiated CH_4, solid NH_4SH includes a strong base, SH^-, and so rapid efficient proton-transfer is expected to reform one of our starting materials.

$$NH_4^{2+} + SH^- \rightarrow NH_3^+ + H_2S \quad (5)$$

An alternative to (5) will be geminate recombination of NH_4^{2+} and e^- to reform excited ammonium (a strong acid), with protonation of the strong base SH^- following to again give H_2S. Subsequent combination of NH_3^+ and e^- will regenerate the other starting material, NH_3. An alternative two-center sequence to these reactions is that excitation of an adjacent ion pair will produce NH_3 and H_2S without radical intermediates:

$$[NH_4^+ \cdots SH^-] \rightarrow [NH_4^+ \cdots SH^-]^* \rightarrow [NH_3 \cdots H_2S] \rightarrow NH_3 + H_2S \quad (6)$$

A similar set of reactions involving ionization and excitation will occur with SH^- to give S atoms and sulfur-containing molecules, ions, and radicals. Such reactions include the formation of atomic sulfur, by H_2S dissociation, followed by a chain-lengthening process such as:

$$S + SH^- \rightarrow HS_2^- \quad \text{or} \quad S + SH^- \rightarrow H^+ + S_2^{2-} \quad (7)$$

The 491 cm^{-1} band identified in our spectra has been attributed to both sulfur products given in (7). Either of the anions formed in (7) could also form the S_3^-· radical we observe at 566 cm^{-1} through a reaction such as:

$$SH + HS_2^- \rightarrow S_3^- + H_2 \quad (8)$$

In addition to ionization of bisulfide, the radical reactant in (8) is the main product formed in low-temperature photolysis of H_2S (Stiles et al., 1966). Multiple studies have also shown that the S_3^-· radical was observed when sulfur is dissolved in liquid NH_3 (Chivers and Lau 1982; Dubois et al., 1987). These same studies also showed the formation of NS_x^-, which we observe at 682 cm^{-1} and one (Dubois et al., 1987) suggested that this anion could form through the reaction:

$$10S + 3NH_3 \rightarrow S_4N^- + 2S_3^- + 3NH_4^+ \quad (9)$$

where S_3^-· is in equibrium with S_6^{2-}. The S_6^{2-} can form in the same manner as described in (7) and can also contribute to the absorption we observed at 491 cm^{-1}.

Besides the reactions described above, the NH_3 produced on irradiation of NH_4SH will be subject to secondary reactions to dissociate it into NH_2, NH, and N. Although dimerization of NH_2 radicals probably occurs to some degree to make N_2H_4, this molecule is difficult to observe *in situ* in our ices due to strong overlapping IR features.

Unfortunately, although these reactions and explanations can be given with reasonable confidence, they lack specificity. Little is known of the relevant reaction energetics or rates, and so it is difficult to specify the dominant mechanistic pathways. More work is needed, and so we currently are carrying out similar radiation studies in the UV and visible regions, where many of these ions have absorption bands.

4.5. Kinetics of radiolytic destruction of amorphous NH_4SH

An important goal of our work is to determine the stability of solid NH_4SH on exposure to ionizing radiation, information needed to assess this compound's stability and chemistry in jovian clouds. Fig. 5 shows kinetics plots for the radiation-induced destruction of NH_4SH at five temperatures, with the most striking aspect of this figure being the differences in the shapes of the curves in the upper and lower panels. This variation implies that different reactions or reaction rates apply to the two different temperature regimes. That the data in the 10–75 K curves reach equilibrium values suggesting that the kinetics are dominated by reversible reactions with at least one temperature-dependent rate constant. The increase in the final value of the normalized band area $\mathcal{A}/\mathcal{A}_0$ on going from 10 to 75 K means that more reactant is present at equilibrium as the reaction temperature rises, suggesting a back reaction that is increasingly efficient. The higher-temperature data, in the upper panel, display a shift from dominance by an equilibrium process to reactions that go to completion, meaning destruction of all NH_4SH initially present. See Espenson (1981) for a description of similar trends in reaction kinetics, especially his Fig. 3-1.

For a more-quantitative analysis of the results in Fig. 5, we adopted a phenomenological approach to write

$$NH_4SH \rightleftharpoons \text{products} \quad (10)$$

with both the forward (destruction) and reverse (reformation) reactions as first order and with rate constants k_1 and k_{-1}, respectively. The corresponding rate expression for the change in [NH_4SH], the concentration of NH_4SH, is

$$-\frac{d[NH_4SH]}{dt} = k_1[NH_4SH] - k_{-1}[\text{products}] \quad (11)$$

which can be solved in the standard manner to give

$$\frac{\mathcal{A}}{\mathcal{A}_0} = \left(1 - \frac{\mathcal{A}_\infty}{\mathcal{A}_0}\right) e^{-(k_1+k_{-1})F} + \frac{\mathcal{A}_\infty}{\mathcal{A}_0} \quad (12)$$

where $\mathcal{A}$ is the integrated absorbance of the IR band used to follow the reaction, 0 and ∞ designate the initial and equilibrium (i.e., time $\rightarrow \infty$) concentrations of NH_4SH, respectively, and proton fluence (F, p+ cm^{-2}) is used instead of irradiation time as the two are proportional. The first and last terms in (12) are the normalized band areas, $\mathcal{A}/\mathcal{A}_0$, that we measured.

Eq. (12) has the form $y = a\,e^{-bx} + c$, where a, b, and c are constants. Table 2 lists values of these constants found by least-squares curve fits to data from NH_4SH irradiations at the five temperatures of

Fig. 5. In the 120 K experiments our initial analysis produced $c < 0$, and so in that case we fitted our destruction curve using $c = 0$. The values of $b = (k_1 + k_{-1})$ are on the order of 10^{-15} cm^2/p+ and can be seen to change by about an order of magnitude between 10 and 120 K. Closer examination shows that b does not vary linearly with temperature but appears to be relatively constant at lower ($\leqslant$75 K) and higher ($\geqslant$100 K) temperatures, reflecting the differences in the decay curves of Fig. 5. Table 2 also shows that c, which is the fraction of NH_4^+ remaining after the sample reached equilibrium, increased slightly with temperature on going from 10 to 75 K, but never attained a uniform, fixed value at the higher temperatures. Turning to the earliest doses, Table 2 also shows that after an irradiation of 1×10^{14} p+ cm^{-2}, the NH_4SH ice was most stable at 120 K, with only 2% being destroyed, with slightly larger destruction at lower temperatures. This trend suggests a somewhat greater efficiency for NH_4SH reformation at higher temperatures and low doses.

An extension of this kinetics analysis would include the formation of secondary radiation products so that Eq. (10) becomes

$$NH_4SH \rightleftharpoons \text{products} \rightarrow \text{secondary products} \quad (13)$$

where the rate constant(s) for forming all such secondary products serves to remove the initially-formed species, such as NH_3 and H_2S, forcing (13) to the right and complete destruction of all NH_4SH, as observed with increasing temperature (see Fig. 5). Although we have not carried out such an analysis we have two strong supporting pieces of evidence for suspecting the non-reversible reaction in (13), evidence represented by our Figs. 9 and 10. Fig. 9 clearly shows that at 120 K, but not 75 K, a process is at work to remove material from the NH_4SH sample. The bursts observed for H_2S^+, NH_3^+, and other ion channels may simply be due to the formation of product molecules, such as H_2S and NH_3, in the irradiated sample followed by their catastrophic release at the higher temperatures. Bursts of temperature, pressure, and materials during irradiation or other energetic processing have been reported for N_2 (Fontana, 1959), H_2O–ice (Shabalin et al., 2003), and CH_4 (Carpenter, 1987), and also on warming ices that were either photolyzed or irradiated (e.g., Moore et al., 1983; Loeffler and Baragiola, 2012). More work is needed to investigate the bursts we observed (Fig. 9) and to evaluate their relevance for NH_4SH and jovian chemistry.

Fig. 10 also offers support for the irreversible step in reaction (13) by showing not just that NH_4SH is lost from our irradiated sample at 120 K, but rather that the ice's thickness also is decreased on prolonged irradiation. Our 2.1-μm sample (B) was selected so that if a thickness decrease occurred during irradiation then there would be an *increase* in the normalized band area, $\mathcal{A}/\mathcal{A}_0$, while with the 1.2-μm sample (A) the opposite would occur. The bottom of Fig. 10 shows that this is exactly what was observed. At low doses the two curves are similar, but at higher ones, when our mass spectrometer indicated that outbursts began (Fig. 9), the two curves diverged. The absorbance for the thicker sample (B) appeared to reach equilibrium and then increased, while the absorbance of the thinner sample (A) continued to fall. In other words, the initial decreases for both samples are from a combination of NH_4SH destruction and a decrease in the ice's thickness. However, in the case of B the integrated absorbance (upper panel) undergoes a somewhat counter-intuitive rise. The overall conclusion is that NH_4SH irradiated at higher temperatures (>∼100 K) experienced greater loss of material than when irradiated at lower temperatures.

Table 2
Radiolytic destruction of amorphous NH_4SH.

T (K)	Amorphous NH_4SH abundance[a]	Fraction left after 1×10^{14} p+ cm^{-2}
120	$1.00 \exp(-0.55 \times 10^{-15} F) + 0.00$[b]	0.98
100	$0.64 \exp(-0.76 \times 10^{-15} F) + 0.36$	0.96
75	$0.26 \exp(-2.83 \times 10^{-15} F) + 0.74$	0.93
50	$0.315 \exp(-4.05 \times 10^{-15} F) + 0.685$	0.89
10	$0.44 \exp(-4.19 \times 10^{-15} F) + 0.56$	0.84

[a] Each entry in the second column is from a least-squares fit of the data to an equation of the form $y = a\ e^{-bF} + c$, where y is the fraction of NH_4SH present after proton fluence F (p+ cm^{-2}), and a, b, and c are constants. See the text for additional information.

[b] Parameter c was set to 0 in this case. Again, see the text for additional information.

4.6. Giant-planet considerations

Theoretical models have long predicted the existence of NH_4SH cloud layers for Jupiter and the other giant planets (Lewis and Prinn, 1970; Weidenschilling and Lewis, 1973; Atreya et al., 1999) and these predictions have received support from spacecraft observations (e.g., Roman et al., 2013). A long-term goal of our laboratory work is to use IR spectroscopy and radiation chemistry to investigate NH_4SH as a jovian cloud and colored aerosol component.

Our experiments predict that a pristine NH_4SH cloud layer near 200 K will contain crystalline NH_4SH since we have observed the amorphous phase of this solid crystallizes quickly above 140 K. However, radiolysis will destroy the crystalline structure of the pristine NH_4SH creating an amorphous mixture of H_2S, NH_3, and probably polysulfides, sulfur anions and ions with N–S bonds. The relative amounts of long-chain sulfur-containing species will likely increase with time in a dynamic situation with cloud ices in a state of sublimation and recondensation. Since some of the expected radiation products are more refractory than NH_3, H_2S, and NH_4SH ices, clouds with such material could be found deep in an atmosphere where temperatures are above those necessary for frozen H_2O, H_2S, NH_3, or NH_4SH to exist. These findings may help to explain some of the discrepancies between measurements (Ragent et al., 1996) and models of giant-planet clouds (Atreya et al., 1997).

An important obstacle in applying our radiation work to gas-giant atmospheres is the lack of information on both radiation sources and doses. Sagan and Khare (1971) pointed out, as did Lewis and Prinn (1970), that breaks in clouds might permit solar-UV photolysis of the deeper NH_4SH regions of Jupiter, but few details were given. Scattergood et al. (1974) studied the bombardment of atmospheric gases by high-energy protons produced by discharges from radiation belts, but again with few details provided. Others have simply and correctly noted that galactic cosmic rays will deliver energy deeper into Jupiter's atmosphere than will solar UV photons (Capone et al., 1979). McDonald et al. (1992) emphasized the importance of auroral processes and electron-induced chemistry, but with a focus on Jupiter's stratosphere, not the region of NH_4SH clouds. Whitten et al. (2008), among others, calculated ionization rates of various jovian-atmospheric molecules by galactic cosmic rays, but all such work appears to have been for the gas phase and not atmospheric solids, ices, or aerosols. More recently, Rimmer et al. (2014) considered the influence of cosmic radiation on gas-giant atmospheres, but the pressures of interest were orders of magnitude too small for the NH_4SH clouds of interest in the present paper. In short, considerable uncertainty remains surrounding radiation doses and dose rates for solid cloud particles. Firmer observations and calculations are needed.

Given the situation just described, we can offer only a very rough estimate for the incident dose rate to a jovian NH_4SH cloud. We adopt the atmospheric cosmic-ray energy flux of 9×10^{-3} ergs cm^{-2} s^{-1} of Sagan and Thompson (1984), which converts to about 6000 MeV cm^{-2} s^{-1}. Our laboratory flux for 0.9 MeV protons is about 1.2×10^{11} MeV cm^{-2} s^{-1} so that 30 min

(fluence $\approx 2 \times 10^{14}$ p+ cm^{-2}) of irradiation in our experiments is roughly 1000 years on Jupiter. Additional insight from observations or theory will be needed to remove numerous uncertainties in this estimate.

Bragin et al. (1977) recognized long ago that the likelihood of resolving mid-IR features of solid NH_4SH in spectra of giant planets is small since the strongest bands are in a region of low solar flux and low thermal emission. However, any such detection could provide information on the local environment of NH_4SH and support the argument that this compound plays a role in giant-planet colors and chemistry.

5. Conclusions

Here we have used infrared spectroscopy to characterize amorphous and crystalline NH_4SH ices. Our results generally agree with the few published spectra available, although quantitative comparisons continue. We also used IR spectroscopy to study the destruction of these samples initiated by 0.9 MeV protons at 10–160 K, observing the formation of NH_3 and products containing nitrogen and sulfur. Crystalline NH_4SH is amorphized by radiation at all temperatures examined, and the amorphization rates have been documented. For amorphous NH_4SH, and consequently the crystalline solid, we estimate that the NH_4^+ solid's initial abundance will drop to about 60% of its original value when irradiated at 10 K and about 80% for a 75-K irradiation. This suggests that with even longer irradiation times (greater doses) and higher temperatures that NH_4^+ and its radiation products should be relatively stable in giant-planet atmospheres. For higher irradiation temperatures, pressure outbursts were observed during irradiation of NH_4SH and likely were due to a build-up and sudden release of radiolytic products in the sample.

Heating irradiated NH_4SH samples showed that their thermal stability is greater than that of unirradiated NH_4SH. This implies that an irradiated giant-planet cloud precipitate containing NH_4SH and these new radiation products can exist at temperatures and altitudes not previously considered. Future laboratory studies will focus on connecting IR results to those obtained from ultraviolet and visible reflectance spectroscopy, which will be more directly comparable to remote-sensing observations of cloud features in the jovian atmosphere.

Acknowledgments

The support of NASA's Planetary Atmospheres and Outer Planets Research programs is gratefully acknowledged. Carly Howett (SWRI, Boulder, Colorado) is thanked for information on her NH_4SH work and for supplying spectral data. Steve Brown, Tom Ward, and Eugene Gerashchenko, members of the NASA Goddard Radiation Effects Facility, operated and maintained the Van de Graaff accelerator.

References

Atreya, S.K. et al., 1997. Chemistry and clouds of Jupiter's atmosphere: A Galileo perspective in Three Galileos: The Man, the Spacecraft, the Telescope. Kluwer Academic Publishers, Dordrecht, pp. 249–260.
Atreya, S.K. et al., 1999. A comparison of the atmospheres of Jupiter and Saturn: Deep atmospheric composition, cloud structure, vertical mixing, and origin. Planet. Space Sci. 47, 1243–1262.
Baratta, G.A., Leto, G., Palumbo, M.E., 2002. A comparison of ion irradiation and UV photolysis of CH_4 and CH_3OH. Astron. Astrophys. 384, 343–349.
Bragin, J., Chang, S., 1976. Photochemistry of ammonium hydrosulfide. Bull. Am. Astron. Soc. 8, 473.
Bragin, J. et al., 1977. Vibrational-spectrum and lattice-dynamics of polycrystalline ammonium hydrosulfide. J. Chem. Phys. 67, 1247–1256.
Briner, E., 1906. Equilibres hétérogénes: Formation du chlorure de phosphonium, du carbamate et du aulfhydrate d'ammoniaque. Compt. Rend. 142, 1416–1418.
Capone, L.A. et al., 1979. Cosmic ray ionization of the jovian atmosphere. Icarus 39, 433–449.
Carpenter, J.M., 1987. Thermally activated release of stored energy in cryogenic media. Nature 330, 358–360.
Chestnut, D.B., 1977. Use of AW2 method for integrated line-intensities from 1st-derivative presentations. J. Magn. Res. 25, 373–374.
Chivers, T., Lau, C., 1982. Raman spectroscopic identification of the S_4N^- and S_3^- ions in blue solutions of sulfur in liquid ammonia. Inorg. Chem. 21, 453–455.
Chivers, T. et al., 1980. Synthesis and crystal and molecular structure of $[(Ph_3P)_2N^+][S_4N^-]$ and the electronic structure of the planar acyclic anion, S_4N^-. J. Am. Chem. Soc. 102, 5773–5781.
Cole, T., 1961. Paramagnetic defects in irradiated NH_4ClO_4. J. Chem. Phys. 35, 1169–1173.
de Pater, I. et al., 2001. Reconciling Galileo probe data and ground-based radio observations of ammonia on Jupiter. Icarus 149, 66–78.
Delitsky, M.L., Baines, K.H., 2007. Jupiter's great red spot: Cloud chemistry and chromophore formation. Bull. Am. Astron. Soc. 39, 444.
Dubois, P., Lelieur, J.P., Lepourte, G., 1987. Chemical species in solutions of sulfur in liquid ammonia. Inorg. Chem. 26, 1897–1902.
Dubois, P., Lelieur, J.P., Lepoutre, G., 1988. Identification and characterization of ammonium polysulfides in solution in liquid ammonia. Inorg. Chem. 27, 1883–1890.
Espenson, J.H., 1981. Chemical Kinetics and Reaction Mechanisms. McGraw-Hill, New York.
Ferraro, J.R., Sill, G., Fink, U., 1980. Infrared intensity measurements of cryodeposited thin films of NH_3, NH_4HS, H_2S, and assignments of absorption bands. App. Spec. 34, 525–533.
Fontana, B.J., 1959. Magnetic study of the frozen products from the nitrogen microwave discharge. J. Chem. Phys. 31, 148–153.
Fujiyama, T., Herrin, J., Crawford, B.L., 1970. Vibrational intensities XXV: Some systematic errors in infrared absorption spectrophotometry of liquid samples. Appl. Optics 24, 9–15.
Howett, C.J.A. et al., 2007. Optical constants of ammonium hydrosulfide ice and ammonia ice. J. Opt. Soc. Am. B – Opt. Phys. 24, 126–136.
Hudson, R.L., Moore, M.H., 2001. Radiation chemical alterations in Solar System ices: An overview. J. Geophys. Res. 106, 33275–33284.
Hudson, R.L., Gerakines, P.A., Moore, M.H., 2014. Infrared spectra and optical constants of astronomical ices: II. Ethane and ethylene. Icarus 243, 147–148.
Huntress Jr., W.T., Anicich, V.G., 1984. Colored sulfur species in the atmosphere of Jupiter. Bull. Am. Astron. Soc. 16, 648.
Hyde, J.S., Freeman, E.S., 1961. E.P.R. observation of NH_3^+ formed by X-ray irradiation of ammonium perchlorate crystals. J. Phys. Chem. 65, 1636–1638.
Isambert, F., 1881. Etude de la vapeur de bisulfhydrate d'ammoniaque. Compt. Rend. 92, 919–922.
Janz, G.J. et al., 1976. Raman studies of sulfur-containing anions in inorganic polysulfides. Sodium polysulfides. Inorg. Chem. 15, 1759–1763.
Lebofsky, L.A., Fegley, M.B., 1976. Laboratory reflection spectra for determination of chemical composition of icy bodies. Icarus 28, 379–387.
Lewis, J.S., Prinn, R.G., 1970. Jupiter's clouds – structure and composition. Science 169, 472–473.
Loeffler, M.J., Baragiola, R.A., 2012. Blistering and explosive desorption of irradiated ammonia–water mixtures. Astrophys. J. 744, 102.
Loeffler, M.J. et al., 2011. Radiolysis of sulfuric acid, sulfuric acid monohydrate, and sulfuric acid tetrahydrate and its relevance to Europa. Icarus 215, 370–380.
Maeda, S., Schatz, P.N., 1961. Absolute infrared intensity measurements in thin films. J. Chem. Phys. 35, 1617–1621.
McDonald, G.D., Thompson, W.R., Sagan, C., 1992. Radiation chemistry in the jovian stratosphere: Laboratory simulations. Icarus 99, 131–142.
Moore, M., Hudson, R., 1992. Far-infrared spectral studies of phase changes in water ice induced by proton irradiation. Astrophys. J. 401, 353–360.
Moore, M.H. et al., 1983. Studies of proton-irradiated cometary-type ice mixtures. Icarus 54, 388–405.
Moore, M.H. et al., 2007. Ammonia–water ice laboratory studies relevant to outer Solar System surfaces. Icarus 190, 260–273.
Pacansky, J., England, C.D., 1986. Analysis of infrared specular reflection spectroscopy for rare-gas matrices. J. Phys. Chem. 90, 4499–4508.
Ragent, B. et al., 1996. Results of the Galileo probe nephelometer experiment. Science 272, 854–856.
Rimmer, P.B., Stark, C.R., Helling, Ch., 2014. Jupiter as a giant cosmic ray detector. Astrophys. J. 787, L25–L29.
Roman, M.T., Banfield, D., Gierasch, P.J., 2013. Saturn's cloud structure inferred from Cassini ISS. Icarus 225, 93–110.
Romanescu, C. et al., 2010. Refractive index measurements of ammonia and hydrocarbon ices at 632.8 nm. Icarus 205, 695–701.
Sagan, C., Khare, B.N., 1971. Experimental jovian photochemistry: Initial results. Astrophys. J. 168, 563–569.
Sagan, C., Thompson, W.R., 1984. Production and condensation of organic gases in the atmosphere of Titan. Icarus 59, 133–161.
Scattergood, T., Lesser, P., Owen, T., 1974. Production of organic molecules by proton irradiation. Nature 100, 247–248.
Shabalin, E. et al., 2003. Experimental studies of spontaneous release of accumulated energy in irradiated ices. Rad. Phys. Chem. 67, 315–319.
Simon-Miller, A.A., Banfield, D., Gierasch, P.J., 2001. An HST study of jovian chromophores. Icarus 149, 94–106.
Steudel, R., 2003. Elemental Sulfur and Sulfur-rich Compounds II. Springer-Verlag, Berlin.

Stiles, D.A. et al., 1966. Photolysis of group 6 hydrides. I. solid H_2S, H_2S_2, and D_2S. Can. J. Chem. 44, 2149–2155.
Strazzulla, G. et al., 1992. Ion-beam-induced amorphization of crystalline water ice. Europhys. Lett. 18, 517–522.
Strycker, P.D. et al., 2011. Jovian chromophore characteristics from multispectral HST images. Icarus 215, 552–583.
Teolis, B.D., Loeffler, M.J., Raut, U., Famá, M., Baragiola, R.A., 2007. Infrared Reflectance Spectroscopy On Thin Films: Interference Effects. Icarus 190, 274–279.
Weast, R.C., Astle, M.J., Beyer, W.H. (Eds.), 1984. CRC Handbook of Chemistry and Physics. CRC Press, Inc., Boca Raton.
Weidenschilling, S.J., Lewis, J.S., 1973. Atmospheric and cloud structures of jovian planets. Icarus 20, 465–476.
West, C.D., 1934. The crystal structures of some alkali hydrosulfides and monosulfides. Zeit. Kristallogr. 88, 97–115.
Whitten, R.C. et al., 2008. Predictions of the electrical conductivity and charging of the cloud particles in Jupiter's atmosphere. J. Geophys. Res. 113, E04001.
Wieser, H. et al., 1969. Vibrational spectra and a force field for H_2S_3 and H_2S_4. Can. J. Chem. 47, 1633–1637.
Wong, M.H. et al., 2015. Fresh clouds: A parameterized updraft method for calculating cloud densities in one-dimensional models. Icarus 245, 273–281.
Ziegler, J.F., 2010. Stopping and Range of Ions in Matter SRIM2010 <http://www.srim.org>.